Cell Metabolism
Resource

In Vivo Mapping of Hydrogen Peroxide and Oxidized Glutathione Reveals Chemical and Regional Specificity of Redox Homeostasis

Simone C. Albrecht,[1] Ana Gomes Barata,[1] Jörg Großhans,[3] Aurelio A. Teleman,[2] and Tobias P. Dick[1,*]
[1]Division of Redox Regulation, DKFZ-ZMBH Alliance, German Cancer Research Center (DKFZ), Im Neuenheimer Feld 280, D-69120 Heidelberg, Germany
[2]Research Group Signal Transduction in Cancer and Metabolism, German Cancer Research Center (DKFZ), Im Neuenheimer Feld 580, D-69120 Heidelberg, Germany
[3]Institute for Biochemistry, Medical School, University of Göttingen, Justus-von-Liebig-Weg 11, D-37077 Göttingen, Germany
*Correspondence: t.dick@dkfz.de
DOI 10.1016/j.cmet.2011.10.010

SUMMARY

The glutathione redox couple (GSH/GSSG) and hydrogen peroxide (H_2O_2) are central to redox homeostasis and redox signaling, yet their distribution within an organism is difficult to measure. Using genetically encoded redox probes in *Drosophila*, we establish quantitative in vivo mapping of the glutathione redox potential (E_{GSH}) and H_2O_2 in defined subcellular compartments (cytosol and mitochondria) across the whole animal during development and aging. A chemical strategy to trap the in vivo redox state of the transgenic biosensor during specimen dissection and fixation expands the scope of fluorescence redox imaging to include the deep tissues of the adult fly. We find that development and aging are associated with redox changes that are distinctly redox couple-, subcellular compartment-, and tissue-specific. Midgut enterocytes are identified as prominent sites of age-dependent cytosolic H_2O_2 accumulation. A longer life span correlated with increased formation of oxidants in the gut, rather than a decrease.

INTRODUCTION

Reactive oxygen species, oxidative stress, and antioxidant levels are widely believed to play key roles in health and disease. For example, oxidants and oxidative changes have been linked to inflammation (Nathan and Ding, 2010) and aging (Finkel and Holbrook, 2000). Oxidants are suspected of causing or exacerbating various disease states either through the damage they may inflict or by inducing alterations in redox-sensitive cell signaling pathways (Houstis et al., 2006; Lin and Beal, 2006). Unfortunately, our knowledge of the redox changes that actually occur in the physiological whole-body context of living animals is extremely limited. We know very little about the redox differences that exist naturally between the different tissues and cell types within the body. It also remains unclear to what extent in vivo redox states are influenced by behavioral and environmental factors, e.g., physical activity, nutrition, or infection. Our lack of knowledge is especially obvious with regard to the exact chemical nature of these changes, their subcellular origin, their spatio-temporal distribution, and their biological relevance.

Most previous redox measurements in animal model organisms have either relied on indirect evidence, e.g., late-stage markers of cellular damage, or have been based on disruptive methods. Oxidative damage markers are considered questionable because damage levels may reflect changes in repair and turnover rather than differential oxidant levels (Murphy et al., 2011). On the other hand, disruptive methods, e.g., the determination of GSH/GSSG ratios by extracting whole organisms or tissues, average over cell types and subcellular compartments. It is, however, very likely that the consideration of tissue-, cell type-, and subcellular compartment-specific redox differences and changes is crucial for our understanding of redox biology.

Another important issue is that no single redox couple or reactive species can be considered representative of all redox processes that occur in a cell at a given instant of time. Cells harbor a variety of redox couples, many of which are far from being in equilibrium with each other, and most have distinct roles and regulation. For example, an increase in glutathione disulfide (GSSG) inside the mitochondrial matrix is likely to have different causes and consequences (and therefore biological meaning) than an increase in cytosolic H_2O_2 concentration. Consequently, it seems expedient to analyze the various redox species specifically and separately, with subcellular resolution on various timescales.

Recent advances in probe development, based on redox-sensitive GFPs (roGFPs) (Dooley et al., 2004; Hanson et al., 2004), now make it possible to work toward the goal of redox couple-specific in vivo imaging at subcellular resolution in model organisms. RoGFPs contain an engineered dithiol/disulfide switch on their surface. The redox equilibrium of the engineered cysteines is associated with measurable ratiometric fluorescent changes. Importantly, the redox-dependent fluorescence ratio exhibited by roGFP2 is insensitive to pH changes in the physiological range (Schwarzlander et al., 2008). It has been established that endogenous cellular

glutaredoxins facilitate equilibration of roGFPs with the glutathione pool (Meyer et al., 2007). Subsequently, we showed that roGFP2 can be directly fused to glutaredoxin (Grx), which increases specificity for glutathione, enhances the kinetics of equilibration between the glutathione and roGFP redox couples, and effectively allows measurement of the glutathione redox potential (E_{GSH}) (Gutscher et al., 2008). Moreover, the fusion to Grx makes the roGFP2 response independent of endogenous Grx. This independence is important because the expression and/or activity of endogenous Grx may differ between cell types, subcellular compartments, developmental stages, and environmental conditions. Importantly, we also recognized that roGFPs can be converted into specific probes for H_2O_2 by coupling them to the microbial H_2O_2 sensor oxidant receptor peroxidase 1 (Orp1) instead of to Grx (Gutscher et al., 2009).

The goal of this work was to undertake steps toward establishing a measuring system that allows monitoring of the actual in vivo status of chemically defined redox species (i.e., the GSH/GSSG redox couple and H_2O_2, respectively) in defined subcellular compartments (i.e., cytosol and mitochondria, respectively) with cellular resolution for the whole body of an animal. To this end, we generated transgenic *Drosophila melanogaster* using four different redox probes to allow measurement of E_{GSH} in the cytosol (cyto-Grx1-roGFP2) and in the mitochondrial matrix (mito-roGFP2-Grx1), and for measuring H_2O_2 in the cytosol (cyto-roGFP2-Orp1) and in the mitochondrial matrix (mito-roGFP2-Orp1). In order to obtain an organism-wide overview, we chose to express these probes ubiquitously through the tubulin promoter. The parallel use of probes for E_{GSH} and H_2O_2 can be considered complementary: while the glutathione redox pair represents a major protection system against oxidants, H_2O_2 is the major oxidant species involved in protein thiol oxidation and redox regulation.

In this study, we present the following findings: First, live imaging of biosensor-transgenic larvae reveals natural redox differences that exist between different cells and tissues. The imaging of living larvae also identifies localized redox changes that occur during physiological transitions such as the cessation of feeding behavior. Second, live redox imaging reveals that the authentic in vivo redox state of the probes can be dependably trapped and conserved by a chemical procedure. Thus, fluorescence-based redox imaging can be applied to dissected animals and becomes available to otherwise optically inaccessible tissues. Third, we identify adult tissues that show either age-dependent or age-independent oxidation. A key insight is that aging-dependent pro-oxidative changes exist but are highly restricted to particular tissues and regions, instead of affecting the whole organism. Midgut enterocytes are major sites of cytosolic H_2O_2 accumulation during aging. Increased life span was accompanied by increased formation of oxidants, rather than by a decrease. Fourth, our measurements suggest that the two oxidant species GSSG and H_2O_2 can change independently of each other. They appear to carry different kinds of biological information and therefore must be measured specifically and separately. Fifth, redox imaging allows investigation of the in vivo influence of individual gene products and pharmacological agents. N-acetyl cysteine (NAC) did not show obvious antioxidative effects in vivo but rather induced an increase in mitochondrial H_2O_2 in various tissues.

RESULTS

Generation of Biosensor-Transgenic Flies

To enable the observation of in vivo redox processes, we created flies broadly expressing either a cytosolic E_{GSH} probe (Tubulin-Gal4, UAS-Grx1-roGFP2), a mitochondrial E_{GSH} probe (Tubulin-Gal4, UAS-mito-roGFP2-Grx), a cytosolic H_2O_2 probe (Tubulin-roGFP2-Orp1), or a mitochondrial H_2O_2 probe (Tubulin-mito-roGFP2-Orp1). In these constructs, Grx1 mediates roGFP2 oxidation by GSSG, and Orp1 mediates roGFP2 oxidation by H_2O_2, respectively (Figures 1A and 1B). The correct subcellular targeting to either cytosol or mitochondria was confirmed by confocal microscopy (see Figure S1 available online). The general in situ response of each probe was tested by exposure of freshly prepared imaginal discs to exogenous reductant (dithiothreitol, DTT) or oxidant (diamide, DA) for 2 min (Figures 1A′ and 1B′). In each case the observed dynamic range between fully reduced and fully oxidized tissues was between 5 and 7 (Figures 1A″ and 1B″).

Tissue-Specific Redox Differences and Changes in Living Larvae

To obtain information about basal redox states and endogenous redox differences between tissues, we performed live imaging of third-instar larvae. We found the cytosolic E_{GSH} probe to be highly reduced throughout the whole larva (Figures 2A and 2A′), close to the lower end of the measuring range, corresponding to −300 mV or less (Meyer and Dick, 2010). There was little variation within and between tissues, as exemplified by measurements on five major tissues (muscle, hemocytes, gut, Malpighian tubules, and fat) (Figures 2A and 2A′ and Figure S2A). In contrast, mitochondrial E_{GSH} was clearly heterogeneous within and between different tissues (Figures 2B and 2B′): while gut enterocytes and muscles were consistently found in a highly reduced state, hemocytes, Malpighian tubules, and fat body tissues showed variation toward a much more oxidized mitochondrial glutathione pool (Figures 2B and 2B′ and Figure S2B, and representative detailed Figure 2C). The cytosolic and mitochondrial H_2O_2 probes also showed significant variation between tissues (Figures 2D, 2D′, 2E, and 2E′). For instance, in both compartments Malpighian tubules exhibited higher H_2O_2 levels than did muscle tissue. Having observed steady-state redox differences in living larvae, we then asked if changes in larval physiology lead to changes in either E_{GSH} or endogenous H_2O_2 levels. To investigate a physiological transition that occurs naturally during larval development, we compared feeding larvae to those that had just stopped feeding and entered the wandering stage. In a highly reproducible manner, the wandering larvae, but not the feeding larvae, exhibited pronounced cytosolic H_2O_2 production within a delimited patch of anterior adipose tissue (Figure 2F, Figures S2C and S2C′). Only minor changes were reported by the mitochondrial H_2O_2 probe and no changes at all by the two E_{GSH} probes (Figures S2D, S2D′, and S2E). Together, these observations show that physiological redox differences and changes can be seen in living larvae and that they are distinct in terms of location, tissue type, subcellular compartment, and redox chemistry.

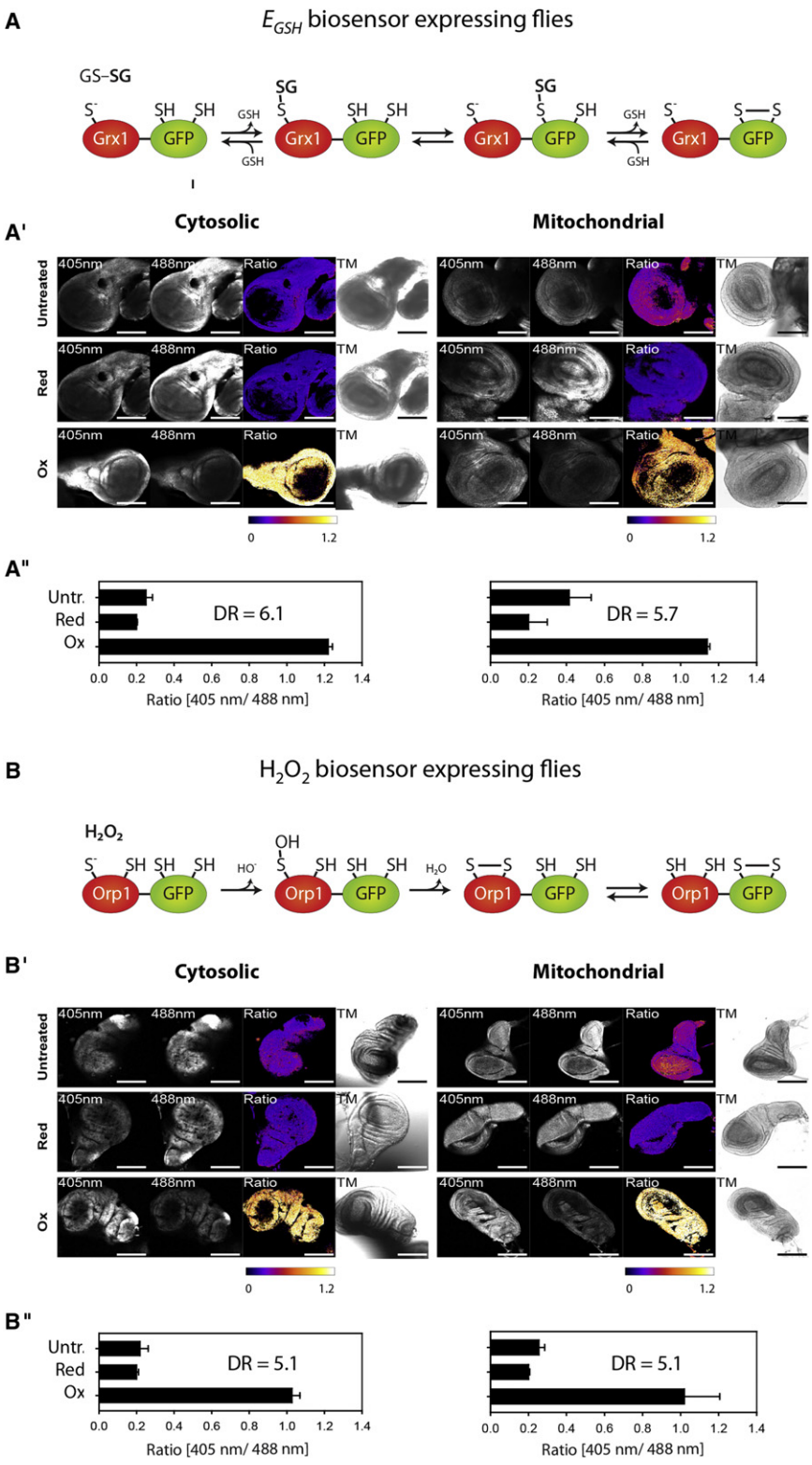

Figure 1. Generation of Biosensor-Transgenic Flies

(A and B) Molecular mechanism of GSSG sensing in Grx1-roGFP2 transgenic flies (A) and of H_2O_2 sensing by roGFP2-Orp1 transgenic flies (B). (A′ and B′) Transgenic lines expressing E_{GSH} probes (A′) or H_2O_2 probes (B′) in either the cytosol or the mitochondrial matrix were tested for in situ responsiveness. All four lines responded as expected to exogenously applied reductant (DTT) and oxidant (DA) as shown for larval wing discs of third-instar larvae. Scale bars, 200 μm (A′) and 250 μm (B′). (A″ and B″) The corresponding dynamic range (DR) is indicated for each probe. Error bars represent the SD of triplicates.

Chemical Conservation of the Biosensor Redox State during Dissection and Fixation

It is important to be able to perform in situ redox measurements not only on the transparent stages of early development but also on adult flies. Therefore, we asked if flies can be dissected and their tissues fixed without perturbing the endogenous state of the redox probes. We expected that from the moment of disruption of organismal integrity (i.e., dissection) tissues will progressively show signs of oxidation over time. However, it was fundamentally unclear how fast the process of tissue oxidation would actually proceed after dissection. To address this question, we imaged larvae before, during, and after dissection. Exemplified by the response of cyto-Grx1-roGFP2 in the midgut (Figure 3A), we generally found a very slow but continuous increase in sensor oxidation that became evident about 10 min after the initiation of dissection. A more detailed time course (Figure 3A′) showed that the redox state in the intact organism (0 min) does not significantly change during and immediately after dissection. Very similar behavior was recorded for mito-roGFP2-Grx1 and both Orp1-based probes. These observations demonstrated that alterations of the sensor redox state after dissection (i.e., in tissues that are not directly damaged) are not immediate but rather require several minutes to show effect. This suggested to us the opportunity to fully prevent artificial probe oxidation by using fast-acting tissue-permeating alkylating agents during the dissection and fixation processes. We observed previously that thiol alkylation of roGFP-based probes fully conserves their redox state and protects them against subsequent oxidation (Gutscher et al., 2008). We reconfirmed in vitro that N-ethyl maleimide (NEM) is a highly effective roGFP2-thiol-blocking agent (Figure 3B) that acts almost instantaneously (Figure 3C) and also protects against thiol oxidation mediated by short- or long-term incubation with paraformaldehyde (PFA)

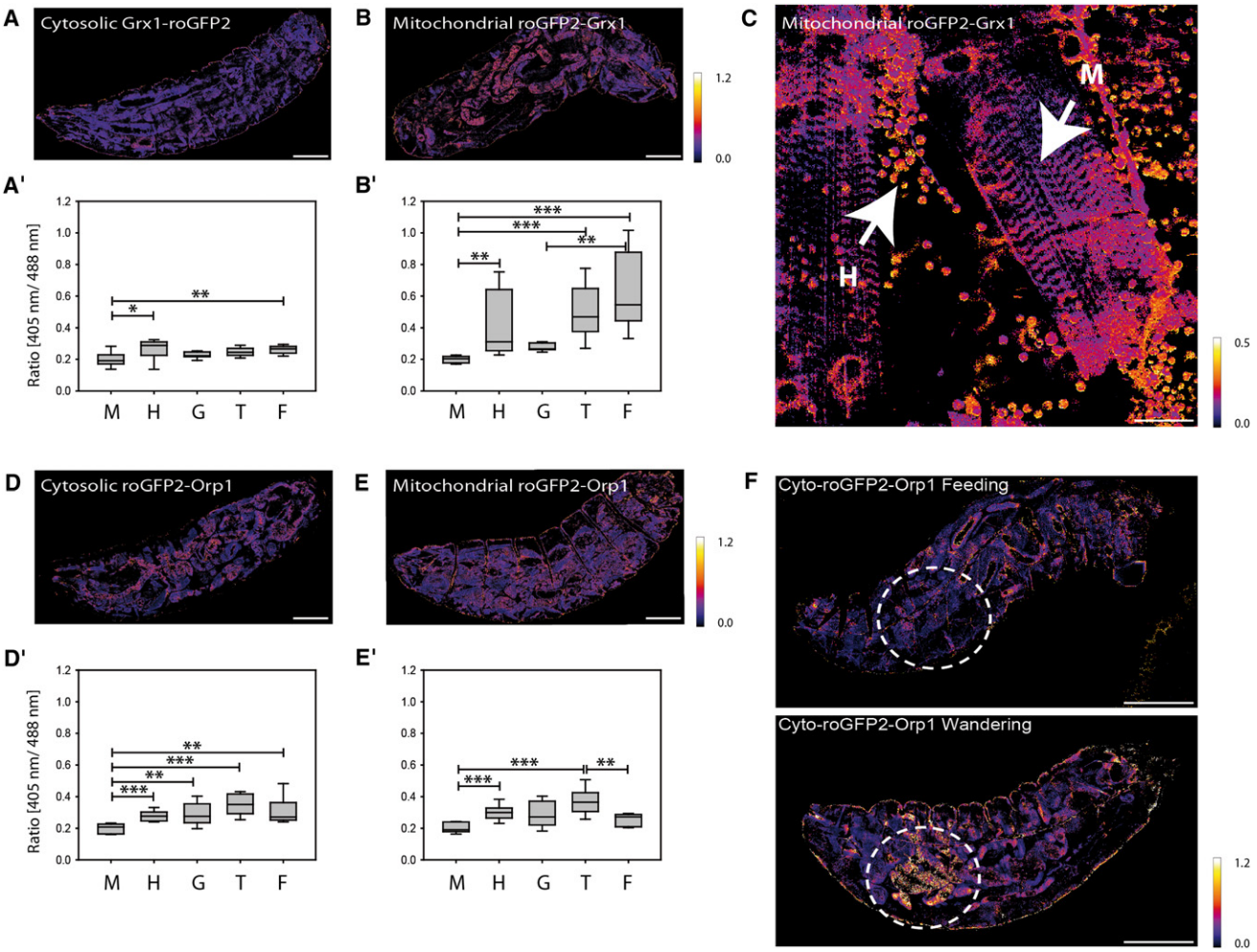

Figure 2. Tissue-Specific Redox Differences and Redox Changes in Living Larvae

(A, B, D, and E) Ratio images of whole intact larvae expressing cyto-Grx1-roGFP2 (A), mito-roGFP2-Grx1 (B), cyto-roGFP2-Orp1 (D), and mito-roGFP2-Orp1 (E). Probe responses in selected tissues were quantified in ten individual third-instar larvae for each biosensor (A′, B′, D′, and E′). Boxes, lower/upper quartile; whiskers, 5th/95th percentile. *$p < 0.05$, **$p < 0.01$, ***$p < 0.001$. M, muscle; H, hemocytes; G, gut; T, (Malpighian) tubules; F, fat. Scale bars, 600 μm. (C) A representative detailed image to highlight tissue-specific differences evident in mito-roGFP2-Grx1-expressing larvae. Arrows indicate hemocytes (H) and muscle tissue (M). Scale bar, 60 μm. (F) Feeding (top) and wandering (bottom) third-instar larvae expressing the cytosolic roGFP2-Orp1 probe. Scale bars, 600 μm.

(Figure 3D). Protection against PFA-mediated oxidation was also confirmed in cell culture experiments (Figure 3E). NEM was then shown to prevent sensor oxidation during tissue preparation and PFA fixation (Figure 3F), the probe redox state being stable even after challenge with high concentrations of the strong thiol oxidant diamide (Figure 3G). In conclusion, dissection in the presence of at least 2 mM NEM is both necessary and sufficient to prevent oxidation artifacts and to allow study of endogenous redox states in dissected larval and adult flies.

Age-Related Redox Changes in the Adult Fly

To address the question of how tissue redox states differ in adult flies and if tissues display pro-oxidative changes during aging, we used the NEM-based fixation technique described in the previous section to analyze various tissues from flies of different age. On the one hand, we found redox differences that exist in young individuals and remain unchanged with increasing age. In particular, abdominal fat tissue is segregated into regions of different morphology (Figures S3A and S3B) which show pronounced differences in mitochondrial H_2O_2 levels in both younger (Figure 4A) and older flies (Figure 4B). No corresponding differences were seen with the mitochondrial E_{GSH} probe (Figure 4C and Figure S3B). On the other hand, age-dependent pro-oxidative changes do exist as well; however, they are not uniformly distributed but rather restricted to particular tissues. Most prominent among the examined tissues, midgut enterocytes exhibit a pronounced age-dependent increase in cytosolic H_2O_2 levels (Figures 4D and 4D′). In this case, a corresponding change in cytosolic E_{GSH} is also detectable which is much less pronounced, yet significant (Figure S3C). We conclude that age-related redox changes are highly nonuniform within the organism and that their detection depends critically on the measured redox species/redox pair, the subcellular compartment, and the tissue/cell type investigated.

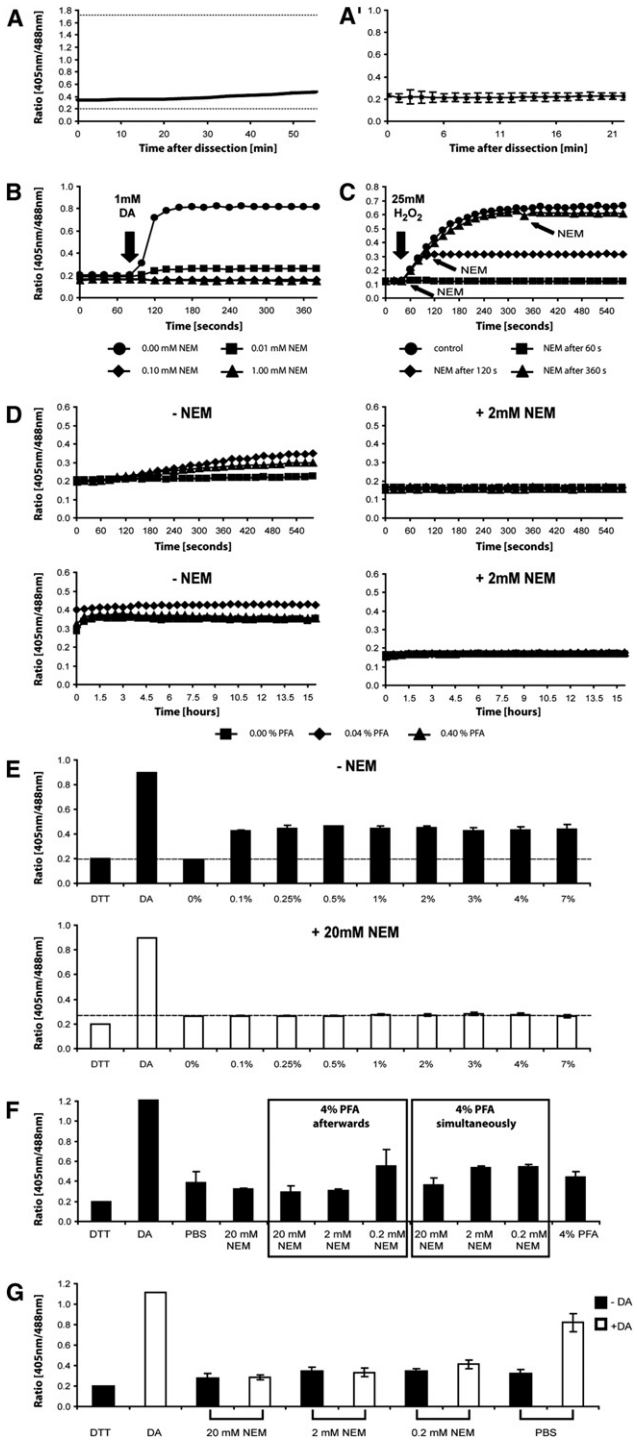

Figure 3. Chemical Conservation of the Biosensor Redox State during Dissection and Fixation

(A) (A and A′) The gut of a third-instar larva expressing cyto-Grx1-roGFP2 was dissected in PBS, then imaged over 55 min (A). Reference lines indicate complete probe reduction (ratio, 0.2) and oxidation (ratio, 1.67), as determined by in situ calibration with DTT and DA, respectively. To obtain a more detailed time course for the first minutes following dissection, larval guts expressing cyto-Grx1-roGFP2 were imaged in intact living larvae (0 min) and then in the same larvae every minute up until 22 min after dissection (A′). Error bars represent the SD (n = 3).

Having observed pronounced age-dependent pro-oxidative changes in midgut enterocytes, we asked about their relationship to life span. First, we compared male and female flies. The median life span of males was shorter by 12 days (Figure 4D″). Despite their shorter life span, males exhibited much less H_2O_2 accumulation in the gut (Figures 4D and 4D′). Second, we examined *chico*$^{1/+}$ flies, which carry a mutation in the insulin/IGF signaling pathway that leads to life span extension (Clancy et al., 2001). We confirmed that the heterozygous *chico*$^{1/+}$ genotype leads to an extension of median life span in females (8 days, Figure 4E′), yet for males we did not record a significant difference (Figure 4F′). We observed that *chico*$^{1/+}$ females showed an accelerated accumulation of cytosolic H_2O_2 in the gut (Figure 4E), while *chico*$^{1/+}$ males showed a delayed accumulation (Figure 4F). Thus, the increase in female life span afforded by *chico*$^{1/+}$ was accompanied by increased rather than decreased formation of oxidants. In conclusion, the generation of H_2O_2 in gut enterocytes does not seem to be a factor in the limitation of life span.

In Vivo Redox Changes Caused by Gene Silencing

To explore the possibilities of combining redox imaging with reverse genetics, we created flies expressing biosensors ubiquitously under the tubulin promoter together with dsRNA constructs expressed specifically in the posterior compartment of the wing disc using engrailed-GAL4. This procedure allows imaging of redox differences side by side between the posterior compartment of the wing disc where a gene of choice is knocked down, compared to the control anterior compartment. Gene silencing of thioredoxin reductase (TrxR) led to increased H_2O_2 levels and increased glutathione oxidation in both the cytosol and mitochondria, as measured with the corresponding probes (Figure 5A). This result is expected, because in *Drosophila* TrxR also acts as the main glutathione reductase (Kanzok et al., 2001) and is targeted to both cytosol and mitochondria (Missirlis et al., 2002). Silencing of ND42, a component of respiratory complex I, led to increased mitochondrial, but not cytosolic,

(B) Reduced recombinant Grx1-roGFP2 was incubated with different NEM concentrations for 80 s and subsequently challenged with 1 mM DA.

(C) H_2O_2 (25 mM) was injected into a solution of reduced recombinant Grx1-roGFP2 after 40 s. NEM (20 mM) was injected after 40, 100, or 340 s.

(D) Different PFA concentrations were injected after 120 s to a solution of reduced Grx1-roGFP2 which was preincubated with either PBS (left panels) or 2 mM NEM (right panels). The Grx1-roGFP2 redox state was monitored for 10 min (upper panels) and for 16 hr following PFA addition (lower panels).

(E) HeLa cells expressing Cyto-Grx1-roGFP2 were preincubated with PBS (upper panel) or 20 mM NEM (lower panel) for 5 min and consecutively fixed with various concentrations of PFA (0%–7%). The resulting redox state of Cyto-Grx1-roGFP2 was analyzed by flow cytometry. The reference lines indicate the ratio of the non-PFA treated control. Data are means ± SD (n = 2).

(F) Freshly dissected guts expressing cytosolic Grx1-roGFP2 were treated with different NEM concentrations (0.2, 2, and 20 mM) for 10 min. PFA (4%) was applied simultaneously with NEM or afterward. The resulting in situ redox state of the probe was determined by microscopy. Data are means ± SD (n = 3).

(G) Larvae were dissected in the presence of different concentrations of NEM (20, 2, 0.2, and 0 mM). Subsequently, prepared guts were challenged with 5 mM DA to quantify the degree of protection against probe oxidation. The resulting in situ redox state of the probe was determined by microscopy. Data are means ± SD (n = 3).

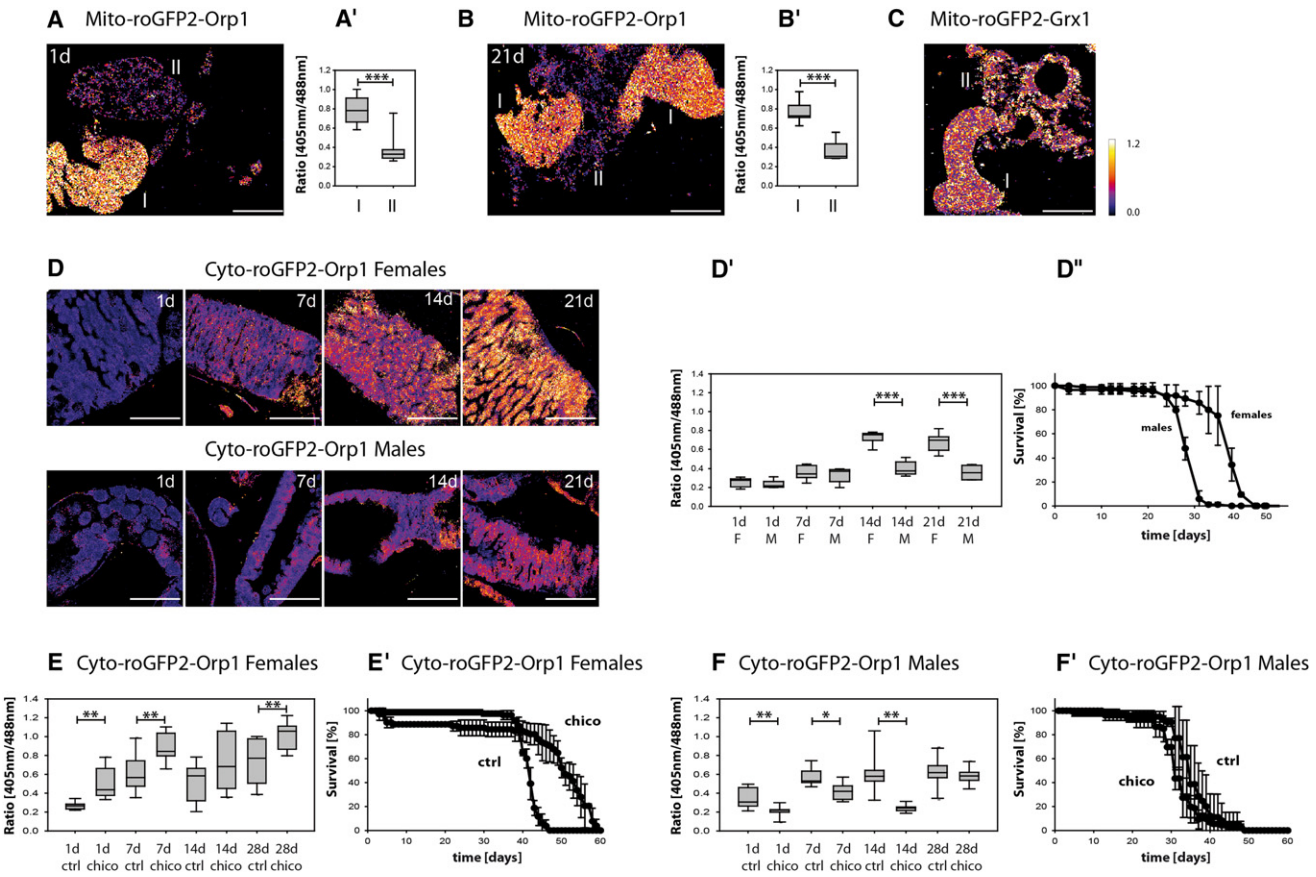

Figure 4. Age-Related Redox Changes in the Adult Fly

(A–C) Fat body tissue of young (A) and old flies (B) expressing mito-roGFP2-Orp1 shows significant age-independent heterogeneity in mitochondrial H_2O_2 levels. No corresponding E_{GSH} difference is reported by the mito-roGFP2-Grx1 probe (C). The two types of fat tissue (labeled I and II) are indicated. Scale bars, 75 μm. ***$p < 0.001$. The false color scale applies to all ratio images in the figure.

(D) Comparison of midgut enterocytes in young (1 day), middle-aged (7 and 14 days), and old flies (21 days) expressing cyto-roGFP2-Orp1 shows a significant age-dependent increase in cytosolic H_2O_2 levels, with females showing a stronger accumulation than males. Quantification using five flies per age and gender (D′), and corresponding life span curve (D″). Scale bars, 150 μm. Boxes, lower/upper quartile; whiskers, 5th/95th percentile. ***$p < 0.001$.

(E and F) Comparison of the age-dependent increase of H_2O_2 levels in gut enterocytes of wild-type and *chico*$^{1/+}$ females (E), and wild-type and *chico*$^{1/+}$ males (F) (1, 7, 14, and 28 days), using ten flies per age for quantification. Boxes, lower/upper quartile; whiskers, 5th/95th percentile. *$p < 0.05$, **$p < 0.01$. Life span curve of wild-type and *chico*$^{1/+}$ females (E′), and of wild-type and *chico*$^{1/+}$ males (F′).

glutathione oxidation (Figure 5B). In contrast, silencing of Jafrac1, the major cytosolic 2-Cys peroxiredoxin, did not show any effects in the posterior wing disc (Figure 5C). However, when Jafrac1 was silenced ubiquitously, using tubulin-GAL4, highly tissue-specific effects were observed, in particular cytosolic accumulation of H_2O_2 and GSSG in the Malpighian tubules (Figures 5D and 5D′). To a lesser extent, mitochondria were also affected (Figure S4). This suggests that silencing of Jafrac1 increases steady-state H_2O_2 levels only in certain tissues and/or physiological conditions. We conclude that redox imaging can be readily combined with genetic approaches to explore the role of gene products on cellular redox states throughout the organism.

In Vivo Redox Changes Caused by Pharmacological Agents

Biosensor transgenic flies offer the opportunity to examine the in vivo influence of pharmacological agents considered to act as oxidants or antioxidants. As an example, we fed larvae with antimycin A, an inhibitor of respiratory complex III, and observed the larval response by live imaging. As expected, in various tissues throughout the larva antimycin A induced mitochondrial (Figure 6A′), but not cytosolic (Figure 6A), probe oxidation. While antimycin A is well understood as an inducer of mitochondrial oxidants, it is much less established if or how small molecule antioxidants influence tissue redox states in vivo. We therefore examined the effect of NAC, one of the most widely used compounds, on larvae and adult flies. Given the common notion that NAC acts as a generic antioxidant, we examined larvae expressing TrxR dsRNA under the engrailed promoter (compare Figure 5A) and asked if NAC feeding would mitigate the oxidative load in the posterior wing disk. However, no significant influence could be detected with either of the two cytosolic probes (Figures S5A and S5A′). We then looked for redox changes in whole larvae by live imaging and also included the

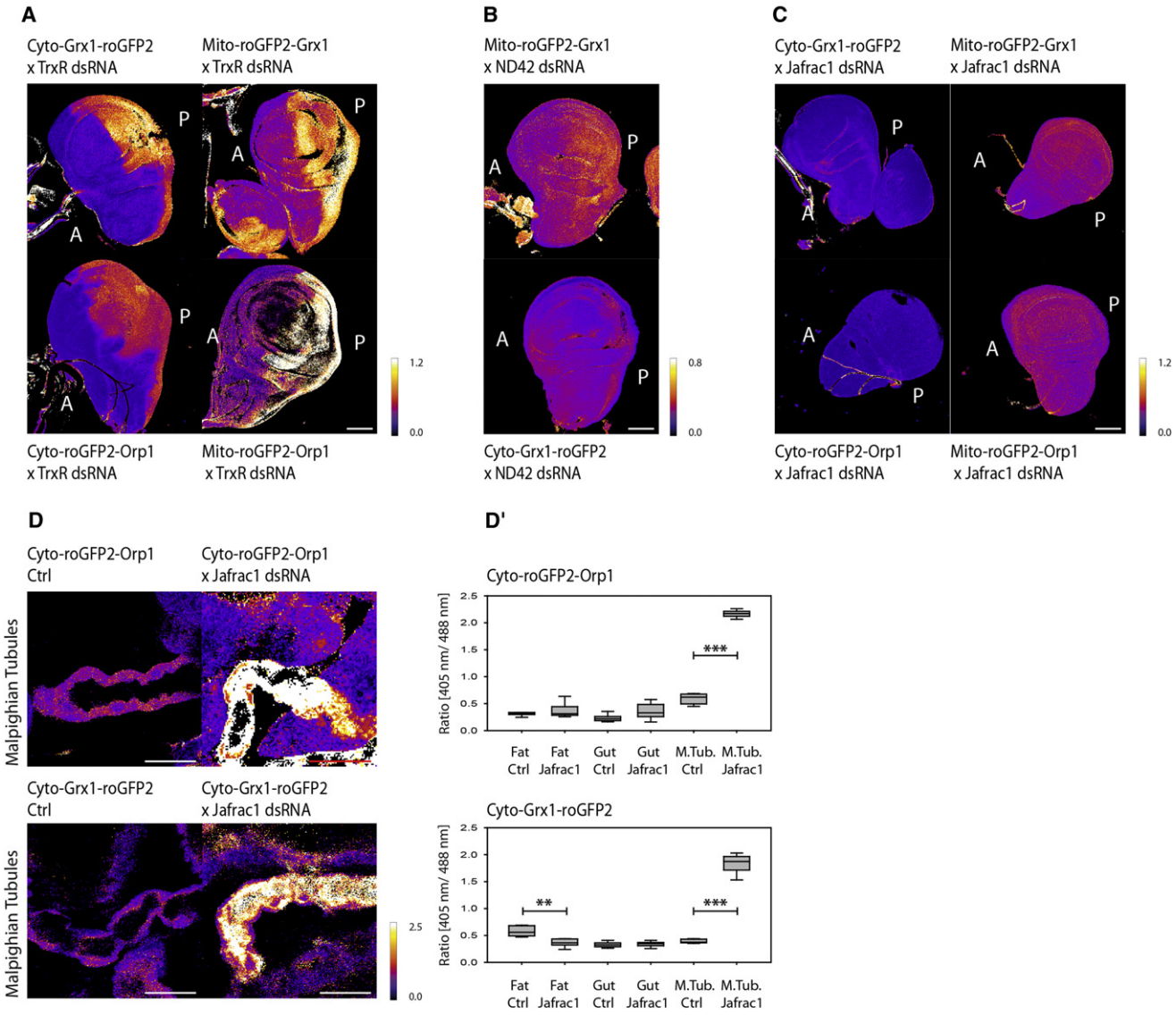

Figure 5. In Vivo Redox Changes Caused by Gene Silencing

(A) Silencing of TrxR in the posterior (P) compartment of the wing disc mediates a pro-oxidative response of all four probes relative to the anterior (A) compartment. Scale bar, 150 μm.

(B) Silencing of complex I subunit ND42 leads to mitochondrial but not cytosolic glutathione oxidation in the posterior part of the wing disc. Scale bar, 150 μm.

(C) Silencing of Jafrac1 in the posterior (P) compartment of the wing disc does not lead to measurable redox changes. Scale bar, 150 μm.

(D) Ubiquitous silencing of Jafrac1 leads to increased cytosolic H_2O_2 and elevated E_{GSH} in Malpighian tubules (M. Tub.). Quantification using five larvae per condition (D′). Scale bars, 75 μm. Boxes, lower/upper quartile; whiskers, 5th/95th percentile. **p < 0.01, ***p < 0.001.

mitochondrial probes. The only significant ($p < 0.01$) NAC-dependent change was an increase in mitochondrial H_2O_2 in various tissues (exemplified for fat and gut tissue in Figure 6B′). The only possible indication of an antioxidant effect, a lowering of cytosolic H_2O_2 levels in the gut (Figure 6B), was of marginal significance ($p = 0.05$). We also extended the NAC feeding experiments to adult flies, which did not show significant changes, except for increased mitochondrial H_2O_2 and GSSG in the Malpighian tubules (Figure S5B). In conclusion, under the conditions tested we did not find convincing evidence for an in vivo antioxidant activity of NAC.

DISCUSSION

In this study we used enzyme-coupled roGFP2-based probes to visualize the in vivo distribution of chemically defined redox species in a transgenic model animal. A key advantage of using genetically encoded redox probes is that they can be precisely targeted to distinct subcellular compartments. Furthermore, ratiometric probes have the benefit of being less prone to a range of common measurement artifacts. Among the genetically encoded ratiometric redox probes, the fluorescent reporter roGFP2 stands out, because its ratiometric signal is insensitive

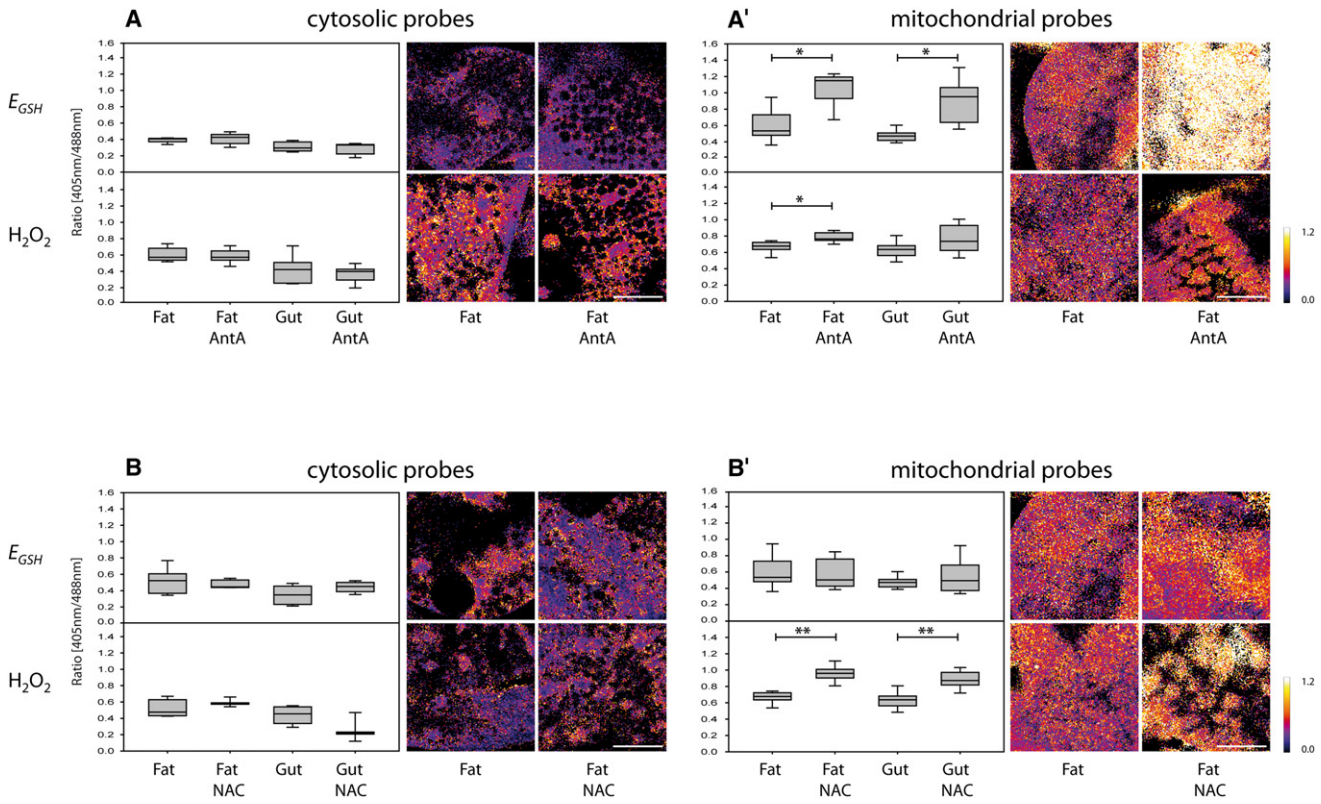

Figure 6. In Vivo Redox Changes Caused by Pharmacological Agents

(A) (A and A′) Live imaging of third-instar larvae that were fed with 10 μg/mL antimycin A for 3 hr. Quantification of all four probes in two representative tissues (fat and gut) using five larvae per condition. Representative images of fat tissue responses. Scale bars, 50 μm. Boxes, lower/upper quartile; whiskers, 5th/95th percentile. *$p < 0.05$.

(B) (B and B′) Live imaging of third-instar larvae that developed from hatching to the L3 stage with food containing 0.1 mg/mL NAC. Quantification of all four probes in two representative tissues (fat and gut) using five larvae per condition. Representative images of fat tissue responses. Scale bars, 50 μm. Boxes, lower/upper quartile; whiskers, 5th/95th percentile. *$p < 0.05$.

to pH in the range between 5.5 and 8.5 (Schwarzlander et al., 2008). Moreover, the response of roGFP2 can be made highly specific for chemically defined oxidants by application of a modular design principle that associates different redox species with the same fluorescent reporter: the oxidoreductase (Grx1)-based probe specifically and reversibly reports roGFP2 oxidation by GSSG, and the peroxidase (Orp1)-based probe specifically and reversibly reports roGFP2 oxidation by H_2O_2. This concept allows comparison of different redox species in different subcellular compartments within the same transgenic system. We find that the two probes show distinct response patterns in vivo, underlining the critical role of the coupled redox enzyme in mediating a sensitive and specific response.

An important step in our study was the establishment and validation of a chemical blocking procedure to prevent artificial oxidation of the redox probes during specimen dissection and fixation, thereby expanding the scope of redox imaging to include the otherwise optically inaccessible parts of the model organism. The procedure is effective because the redox species under consideration (H_2O_2 and GSH/GSSG) do not change immediately upon dissection, but rather it takes several minutes until measurable effects take place. This time window can be exploited to trap the probe redox state with the alkylating agent NEM, which is applied during dissection and permeates exposed tissues within seconds. A combined alkylation-fixation technique thus allows in situ analysis of the in vivo redox state in tissues otherwise inaccessible for direct optical imaging. Thus, the in vivo measurements reported in this study are based on a unique combination of probe features: genetic encoding with specific subcellular targeting, defined oxidant specificity, amenability to instant trapping of the redox state, and pH-insensitive ratiometric reporting.

The almost uniform probe expression obtained under a tubulin promoter allowed us to make a number of general biological observations which have implications regarding the robustness of redox homeostasis, redox compartmentalization, and the relationship between H_2O_2 and E_{GSH}. Throughout the living organism, the cytosolic E_{GSH} is very close to the lower end of the roGFP2 measuring range, which corresponds to a glutathione redox potential between −300 and −320 mV (Meyer and Dick, 2010). This value is very similar to that obtained for other eukaryotes, including yeast (Braun et al., 2010; Ostergaard et al., 2004), *Arabidopsis* (Meyer et al., 2007), and human cells (Gutscher et al., 2008). It is therefore likely that a cytosolic steady-state E_{GSH} in this range is a general feature of eukaryotes, possibly because a less negative potential would drive toxic levels of

cytosolic protein thiol oxidation (Lopez-Mirabal and Winther, 2007). We observed very little variation of cytosolic E_{GSH} in either larvae or in young or old adults. Thus, cytosolic glutathione redox homeostasis in vivo appears to be very robust and stably maintained with increasing age. The stability of cytosolic E_{GSH} in living *Drosophila* contrasts with the observation that cultured mammalian tumor cells show long-lived pro-oxidative changes in cytosolic E_{GSH} depending on cell density, nutrient availability, and other factors (Gutscher et al., 2008). These observations may indicate that cytosolic glutathione redox homeostasis is more stable or restricted in vivo than it is in a cell culture system under ex vivo conditions. However, in contrast to cytosolic E_{GSH}, mitochondrial E_{GSH} was found to be much more variable and dynamic, likely reflecting the fact that mitochondria are major generators of endogenous oxidants (Murphy, 2009). The observed in vivo differences between cytosolic and mitochondrial E_{GSH} are also compatible with the notion that cytosolic and mitochondrial glutathione pools are independently regulated (Hu et al., 2008).

The comparison between Grx- and Orp-based probes also supports the conjecture that changes in E_{GSH} and H_2O_2 levels are not necessarily coupled and concurrent. For example, the high levels of mitochondrial H_2O_2 within patches of adult adipose tissue do not translate into any measurable increases in mitochondrial E_{GSH} (Figures 4A–4C). Likewise, the local increase in cytosolic H_2O_2 that was evident in wandering larvae (Figure 2F) was not associated with a change in cytosolic E_{GSH} (Figure S2E). The explanation may be that in these situations H_2O_2 is predominantly metabolized by thioredoxin-coupled peroxidases, rather than being converted to GSSG. Alternatively, it may be that GSSG is so efficiently reduced (or excreted) that cytosolic E_{GSH} is maintained despite increased rates of glutathione oxidation. Taken together, it seems that H_2O_2 measurements do not necessarily inform about the state of the glutathione system and vice versa. Accordingly, different redox species likely convey different kinds of biological information, and this may hold true for most other oxidant species and redox couples, including $O_2^{\bullet -}$, NO, and NAD^+/NADH, suggesting that one needs to measure all these species separately and specifically with cellular and subcellular compartment resolution.

Knowledge about defined oxidants in defined locations should help to address the complex relationships between oxidants and various other phenomena. A controversial issue is the nature of the relationship between oxidants and aging. It is generally believed that pro-oxidative changes occur during aging. Redox measurements performed on whole flies support the idea, for both GSH/GSSG (Rebrin et al., 2004) and H_2O_2 (Cocheme et al., 2011). However, it is not clear if such changes occur over the whole organism or if they are restricted to particular tissues, regions, and cell types. Our approach allows the identification of tissues, cells, and subcellular compartments which undergo oxidation during aging in vivo. For *Drosophila* we have found that age-dependent pro-oxidative changes are highly restricted to particular locations, with the most prominent change being an increase of cytosolic H_2O_2 in midgut enterocytes. Based on this observation, we asked if and how the rate of H_2O_2 accumulation would be different in flies exhibiting a different life span. In two separate experiments ($chico^{1/+}$ females versus control females, and control females versus control males), increased life span was accompanied by increased formation of oxidants, rather than by a decrease. Thus, in this particular setting our results do not support the idea that aging-related oxidative processes limit life span. It is nevertheless likely that the oxidative phenomena we observe are causally connected to some biological function, possibly to an innate immune response (Ha et al., 2005), driven by an increase in bacterial load in the gut known to accompany aging without life span trade-off (Ren et al., 2007). In this case the observed increase in H_2O_2 levels in enterocytes would probably represent an epiphenomenon of aging rather than a driving force for the aging process. It is generally conceivable that age-related oxidant increases are mostly or largely epiphenomena (Gems and Doonan, 2009).

To proceed beyond correlations and to uncover causal relationships and biological meaning, it will be important not just to observe and quantify particular redox changes but also to manipulate (i.e., prevent/enhance) them in vivo, in a highly specific manner. The approach presented here allows the quantification of the actual in vivo influence of pharmacological or genetic interventions on local H_2O_2 levels or E_{GSH}. This information is crucial for the development of strategies to specifically manipulate in vivo redox states. However, our results also suggest that truly specific and predictable in vivo redox manipulations may be much more difficult to achieve than commonly acknowledged. For instance, silencing of the major cytosolic 2-Cys peroxiredoxin Jafrac-1 had a pro-oxidative effect in some tissues but not in others. Moreover, NAC did not show obvious antioxidative effects in vivo, but rather induced elevated mitochondrial oxidant production in various tissues. Our experiments suggest that the widely held assumption that NAC acts as a generic antioxidant should be treated with caution. Nevertheless, it should be noted that measurements of E_{GSH} do not exclude the possibility that NAC increased total cytosolic GSH levels, and it is furthermore possible that NAC acts as a thiol redox modulator without acting as an antioxidant (Murphy et al., 2011; Parasassi et al., 2010). Taken together, the in vivo effects caused by genetic manipulation of individual redox enzymes or by treatment with small molecule antioxidants may not always meet expectations and may differ widely depending on tissue type, metabolic context, and other factors. Thus, it seems important to clarify if a chosen antioxidant actually reacts with the relevant oxidant in the relevant location inside the organism. Conversely, if an antioxidant shows a biological effect, it remains to be shown that it really lowers oxidant levels rather than acting through other mechanisms. It seems that a significant amount of work, exploiting in vivo probes, will be required before individual oxidant species and redox pairs can be specifically manipulated in vivo with some confidence. In conclusion, many of the observations we report could not have been predicted a priori and therefore highlight the importance of monitoring redox states in vivo.

EXPERIMENTAL PROCEDURES

Genetics

Transgenic *Drosophila melanogaster* were generated by germline injection into a w^{1118} strain. Flies were raised at 25°C on standard medium. Gal4 driver strains were obtained from Bloomington (enGal4 #30564, tubGal4 #5138). In vivo gene knockdowns were performed using dsRNA lines from the Vienna

Drosophila RNAi Center (TrxR, GD 47308; ND42, GD 14444; Jafrac1, KK 109514). For dsRNA-mediated knockdown in the posterior wing disc and ubiquitous sensor expression, enGal4 (II); Tubulin-Sensor (III) lines were crossed with UAS-dsRNA flies. Ubiquitous sensor expression and ubiquitous Jafrac1 knockdown was achieved in flies simultaneously bearing Tubulin-GAL4, UAS-Sensor, and UAS-Jafrac1-dsRNA.

Aging Experiments

All aging experiments were performed at 29°C. To avoid influences of markers or balancers, biosensor-expressing males were crossed to w^{1118} virgins to obtain progeny heterozygous for the biosensor. First-instar larvae were collected from apple agar plates (20% apple juice, 80% PBS, 1% agar, 0.23% Tegosept) and transferred to vials containing food to ensure simultaneous eclosion. Male and female flies were housed together for the first 24 hr after eclosion. Subsequently, males and fertilized females were collected and housed separately. The flies were flipped every 2–3 days. To analyze flies of different ages (1, 7, 14, and 21 days) on the same day for side-by-side comparisons under identical microscopy conditions, separate populations of aging flies were set up under identical conditions with corresponding time delays. For aging experiments with $chico^{1/+}$ flies, biosensor-expressing males were crossed to w^{1118} or *chico* virgin females to obtain sensor/+ or sensor/$chico^{1}$ flies, respectively. One-, seven-, fourteen-, and twenty-eight-day-old flies were compared side-by-side with the same microscope settings.

Feeding of Third-Instar Larvae and Adult Flies with Antimycin A and NAC

To study the influence of antimycin A, third-instar larvae were removed from the food vial, washed briefly with PBS, and transferred to a vial containing food supplemented with 10 μg/mL antimycin A. After 3 hr, living larvae were imaged as described below. To study the influence of NAC, egg-laying adult females where transferred to vials containing food with either 0.1 mg/mL or 1 mg/mL NAC. Third-instar larvae developing in the presence of 0.1 mg/mL NAC were analyzed by live imaging as described below. Likewise, third-instar larvae expressing UAS-TrxR-dsRNA with enGal4 were allowed to develop in food containing 1 mg/mL NAC. Wing discs were prepared and imaged immediately as described below. In addition, freshly eclosed adult flies were housed for 48 hr with food containing 1 mg/mL NAC, followed by dissection and fixation as described below.

Live Imaging of Third-Instar Larvae

Living third-instar larvae were removed from the food vial, cleaned briefly with PBS, and gently fixed with adhesive tape on a cover glass. Larvae were imaged immediately using a Leica TCS SP5 AOBS confocal microscope system (Leica Microsystems) with a HCX PL APO lambda blue 20× 0.7 NA objective (oil immersion) and Leica LAS AF software. Excitation of biosensor fluorescence by the 405 nm and 488 nm laser lines was performed sequentially and line by line. Emission was detected at 500–570 nm. For calibration of the biosensor response, larvae were subsequently dissected in PBS and salivary glands incubated with 10 mM DTT (5′) or 1 mM DA (2′) at room temperature, respectively. The ratio of fully reduced sample was set to 0.2.

Imaging of Freshly Dissected Tissue

To examine larval organs, e.g., the wing disc or salivary glands, organs were freshly dissected in PBS and transferred immediately to a Zeiss LSM 710 ConfoCor 3 microscope equipped with an EC Plan N DICI 40× 1.3 NA objective (oil immersion). Probe fluorescence was excited sequentially at 405 and 488 nm (line by line) and detected at 500–530 nm. TMRM staining was visualized by excitation at 561 nm and by emission at 580–650 nm. For freshly dissected wing discs, a 10× EN Plan N DICI 10×/0.3 NA dry objective was used. To fully reduce and oxidize the tissue, the dissected organs were incubated in 10 mM DTT (5′) or 1 mM DA (2′), respectively. For consistency, we set the ratio of fully reduced organs to 0.2.

Conservation of the Biosensor Redox State with NEM

To conserve the redox state of roGFP2-based biosensors in dissected and fixed tissue, all dissections were performed in the presence of 20 mM NEM. Adult flies were briefly anaesthetized with N_2 and decapitated. The abdomen was cut and opened immediately in the presence of 20 mM NEM. All samples were further incubated with NEM for 10 min at RT. Remaining NEM was removed by rinsing once with PBS. Afterward, samples were fixed with 4% PFA for 15 min at RT. Remaining PFA was removed by washing twice with PBS for 10 min. Samples were equilibrated in glycerol mounting medium (80% glycerol, 0.4% N-propyl gallate in PBS) overnight at 4°C and mounted the next day. Samples were stored horizontally at 4°C. For probe calibration, parallel measurements (side by side, keeping the exact same microscope settings) were performed on specimens that were fully reduced or fully oxidized (20 mM DTT or 2 mM DA for 10 min) during dissection and before being blocked with NEM. This allows determination of the in situ dynamic range and to infer the degree of oxidation of the probe in the actual samples.

Imaging of Fixed Tissue

Fixed tissues were imaged with a Zeiss LSM 710 ConfoCor 3 confocal microscope equipped with an EC Plan N DICI 40×, 1.3 NA objective (oil immersion). Probe fluorescence was excited sequentially at 405 and 488 nm (line by line) and detected at 500–530 nm. Nuclear stain To-Pro3 was excited at 633 nm and detected at 650–700 nm.

Image Processing

Images were saved as 16-bit tif files and processed by ImageJ. Background was subtracted using the rolling ball procedure set to 50 pixels. Pictures were then converted to 32-bit format. The intensities of the 488 nm image were thresholded, and values below threshold were set to "not a number" (NaN). A ratio image was created by dividing the 405 nm image by the 488 nm image pixel by pixel and displayed in false colors using the lookup table "Fire."

In Vitro Experiments

Recombinant Grx1-roGFP2 and roGFP2-Grx1 were expressed in the *E. coli* strain BL21 (Stratagene) and purified via hexahistidine affinity chromatography. Purified recombinant proteins were desalted using Slide-a-Lyzer dialysis cassettes (Pierce). For measurements in a FLUOstar Omega platereader (BMG Labtech), the proteins were diluted into a degassed standard reaction buffer (100 mM phosphate, 5 mM EDTA [pH 7.0]) to a final concentration of 1 μM. RoGFP2 emission was detected (505–515 nm) after excitation at 390 and 480 nm. The ratio 390 nm/480 nm was calculated and plotted against time. For oxidation experiments, roGFP2 fusion proteins were first reduced with 10 mM DTT for 20 min on ice and desalted with Zeba Desalt spin columns (Pierce). To compare between experiments, the ratio of fully reduced protein was set to 0.1.

Cell Culture and FACS Analysis

HeLa cells were grown in DMEM (GIBCO) supplemented with 10% FCS, 2 mM L-glutamine, 100 U/ml penicillin, and 100 mg/ml streptomycin (GIBCO). HeLa cells stably expressing Grx1-roGFP2 were generated by retroviral transduction and subsequent selection with 0.5 mg/ml puromycin. For FACS analysis, cells were pretreated with 20 mM NEM for 5 min at RT, washed once with PBS, and incubated for 5 min with different PFA concentrations. After washing twice with PBS, cells were stored at 4°C. We used a BD FACSAria flow cytometer equipped with 407 and 488 nm lasers for excitation and detected the emission with a standard GFP filter (515–545 nm).

Statistical Analysis

For multiple comparisons, data points were analyzed with one-way analysis of variance (ANOVA), in conjunction with the Tukey range test. To obtain p values for pairwise comparisons, a two-sided heteroscedastic t test was performed. Experimental data were visualized by box plot, showing lower quartile (bottom of box), upper quartile (top of box), median (band near the middle of the box), the fifth percentile (lower end of whisker), and the ninety-fifth percentile (upper end of whisker). Stars indicate p values as obtained from pairwise (t test) comparisons: *$p < 0.05$; **$p < 0.01$; ***$p < 0.001$.

SUPPLEMENTAL INFORMATION

Supplemental Information includes five figures, Supplemental Experimental Procedures, and Supplemental References and can be found with this article online at doi:10.1016/j.cmet.2011.10.010.

ACKNOWLEDGMENTS

This work was financially supported by a grant from the Network Aging Research of the Baden-Württemberg Foundation (to T.P.D.). We thank Dr. Felix Bestvater and Manuela Brom from the DKFZ Light Microscopy Facility for professional microscopy support, Thomas Hielscher from the DKFZ Division of Biostatistics for guidance with statistical analysis, Dr. Bruce Edgar and Dr. Parthive Patel for experimental support and advice, Dr. Cristina Pallares for helpful discussions, Martina Kegel and Jessica Wojtarowic for help with the preparation of figures and the manuscript, and Dr. Bruce Morgan for critical reading of the manuscript.

Received: May 10, 2011
Revised: September 23, 2011
Accepted: October 17, 2011
Published online: November 17, 2011

REFERENCES

Braun, N.A., Morgan, B., Dick, T.P., and Schwappach, B. (2010). The yeast CLC protein counteracts vesicular acidification during iron starvation. J. Cell Sci. *123*, 2342–2350.

Clancy, D.J., Gems, D., Harshman, L.G., Oldham, S., Stocker, H., Hafen, E., Leevers, S.J., and Partridge, L. (2001). Extension of life-span by loss of CHICO, a Drosophila insulin receptor substrate protein. Science *292*, 104–106.

Cocheme, H.M., Quin, C., McQuaker, S.J., Cabreiro, F., Logan, A., Prime, T.A., Abakumova, I., Patel, J.V., Fearnley, I.M., James, A.M., et al. (2011). Measurement of H(2)O(2) within living Drosophila during aging using a ratiometric mass spectrometry probe targeted to the mitochondrial matrix. Cell Metab. *13*, 340–350.

Dooley, C.T., Dore, T.M., Hanson, G.T., Jackson, W.C., Remington, S.J., and Tsien, R.Y. (2004). Imaging dynamic redox changes in mammalian cells with green fluorescent protein indicators. J. Biol. Chem. *279*, 22284–22293.

Finkel, T., and Holbrook, N.J. (2000). Oxidants, oxidative stress and the biology of ageing. Nature *408*, 239–247.

Gems, D., and Doonan, R. (2009). Antioxidant defense and aging in C. elegans: is the oxidative damage theory of aging wrong? Cell Cycle *8*, 1681–1687.

Gutscher, M., Pauleau, A.L., Marty, L., Brach, T., Wabnitz, G.H., Samstag, Y., Meyer, A.J., and Dick, T.P. (2008). Real-time imaging of the intracellular glutathione redox potential. Nat. Methods *5*, 553–559.

Gutscher, M., Sobotta, M.C., Wabnitz, G.H., Ballikaya, S., Meyer, A.J., Samstag, Y., and Dick, T.P. (2009). Proximity-based protein thiol oxidation by H2O2-scavenging peroxidases. J. Biol. Chem. *284*, 31532–31540.

Ha, E.M., Oh, C.T., Bae, Y.S., and Lee, W.J. (2005). A direct role for dual oxidase in Drosophila gut immunity. Science *310*, 847–850.

Hanson, G.T., Aggeler, R., Oglesbee, D., Cannon, M., Capaldi, R.A., Tsien, R.Y., and Remington, S.J. (2004). Investigating mitochondrial redox potential with redox-sensitive green fluorescent protein indicators. J. Biol. Chem. *279*, 13044–13053.

Houstis, N., Rosen, E.D., and Lander, E.S. (2006). Reactive oxygen species have a causal role in multiple forms of insulin resistance. Nature *440*, 944–948.

Hu, J., Dong, L., and Outten, C.E. (2008). The redox environment in the mitochondrial intermembrane space is maintained separately from the cytosol and matrix. J. Biol. Chem. *283*, 29126–29134.

Kanzok, S.M., Fechner, A., Bauer, H., Ulschmid, J.K., Muller, H.M., Botella-Munoz, J., Schneuwly, S., Schirmer, R., and Becker, K. (2001). Substitution of the thioredoxin system for glutathione reductase in Drosophila melanogaster. Science *291*, 643–646.

Lin, M.T., and Beal, M.F. (2006). Mitochondrial dysfunction and oxidative stress in neurodegenerative diseases. Nature *443*, 787–795.

Lopez-Mirabal, H.R., and Winther, J.R. (2007). Redox characteristics of the eukaryotic cytosol. Biochim. Biophys. Acta. *1783*, 629–640.

Meyer, A.J., and Dick, T.P. (2010). Fluorescent protein-based redox probes. Antioxid. Redox Signal. *13*, 621–650.

Meyer, A.J., Brach, T., Marty, L., Kreye, S., Rouhier, N., Jacquot, J.P., and Hell, R. (2007). Redox-sensitive GFP in Arabidopsis thaliana is a quantitative biosensor for the redox potential of the cellular glutathione redox buffer. Plant J. *52*, 973–986.

Missirlis, F., Ulschmid, J.K., Hirosawa-Takamori, M., Gronke, S., Schafer, U., Becker, K., Phillips, J.P., and Jackle, H. (2002). Mitochondrial and cytoplasmic thioredoxin reductase variants encoded by a single Drosophila gene are both essential for viability. J. Biol. Chem. *277*, 11521–11526.

Murphy, M.P. (2009). How mitochondria produce reactive oxygen species. Biochem. J. *417*, 1–13.

Murphy, M.P., Holmgren, A., Larsson, N.G., Halliwell, B., Chang, C.J., Kalyanaraman, B., Rhee, S.G., Thornalley, P.J., Partridge, L., Gems, D., et al. (2011). Unraveling the biological roles of reactive oxygen species. Cell Metab. *13*, 361–366.

Nathan, C., and Ding, A. (2010). Nonresolving inflammation. Cell *140*, 871–882.

Ostergaard, H., Tachibana, C., and Winther, J.R. (2004). Monitoring disulfide bond formation in the eukaryotic cytosol. J. Cell Biol. *166*, 337–345.

Parasassi, T., Brunelli, R., Costa, G., De Spirito, M., Krasnowska, E., Lundeberg, T., Pittaluga, E., and Ursini, F. (2010). Thiol redox transitions in cell signaling: a lesson from N-acetylcysteine. ScientificWorldJournal *10*, 1192–1202.

Rebrin, I., Bayne, A.C., Mockett, R.J., Orr, W.C., and Sohal, R.S. (2004). Free aminothiols, glutathione redox state and protein mixed disulphides in aging Drosophila melanogaster. Biochem. J. *382*, 131–136.

Ren, C., Webster, P., Finkel, S.E., and Tower, J. (2007). Increased internal and external bacterial load during Drosophila aging without life-span trade-off. Cell Metab. *6*, 144–152.

Schwarzlander, M., Fricker, M.D., Muller, C., Marty, L., Brach, T., Novak, J., Sweetlove, L.J., Hell, R., and Meyer, A.J. (2008). Confocal imaging of glutathione redox potential in living plant cells. J. Microsc. *231*, 299–316.